

PAPER

Anisotropic compliance of robot legs improves recovery from swing-phase collisions

To cite this article: Henry Chang *et al* 2021 *Bioinspir. Biomim.* **16** 056001

View the [article online](#) for updates and enhancements.



IOP | ebooks™

Bringing together innovative digital publishing with leading authors from the global scientific community.

Start exploring the collection—download the first chapter of every title for free.

Bioinspiration & Biomimetics



PAPER

Anisotropic compliance of robot legs improves recovery from swing-phase collisions

RECEIVED
15 January 2021

REVISED
4 June 2021

ACCEPTED FOR PUBLICATION
15 June 2021

PUBLISHED
12 August 2021

Henry Chang¹, Justin Chang¹, Glenna Clifton²  and Nick Gravish^{1,*} 

¹ Department of Mechanical and Aerospace Engineering, University of California San Diego, 9500 Gilman Dr, La Jolla, CA 92093, United States of America

² Department of Biology, University of Portland, 5000 N Willamette Blvd, Portland, OR 97203, United States of America

* Author to whom any correspondence should be addressed.

E-mail: ngravish@eng.ucsd.edu

Keywords: legged robots, compliance control, unstructured ground, legged locomotion

Supplementary material for this article is available [online](#)

Abstract

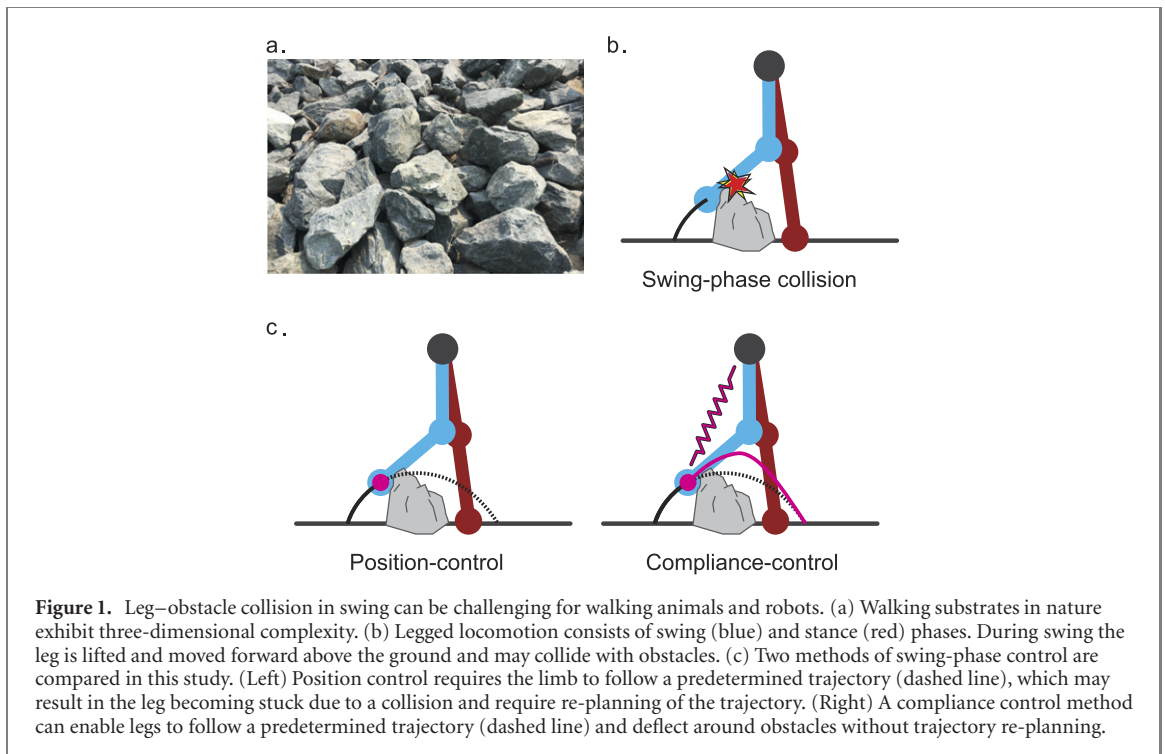
Uneven terrain in natural environments challenges legged locomotion by inducing instability and causing limb collisions. During the swing phase, the limb releases from the ground and arcs forward to target a secure next foothold. In natural environments leg–obstacle collisions may occur during the swing phase which can result in instability, and may require contact sensing and trajectory re-planning if a collision occurs. However, collision detection and response often requires computationally- and temporally-expensive control strategies. Inspired by low stiffness limbs that can pass past obstacles in small insects and running birds, we investigated a passive method for overcoming swing-collisions. We implemented virtual compliance control in a robot leg that allowed us to systematically vary the limb stiffness and ultimately its response to collisions with obstacles in the environment. In addition to applying a standard positional control during swing motion, we developed two virtual compliance methods: (1) an isotropic compliance for which perturbations in the x and y directions generated the same stiffness response, and (2) a vertical anisotropic compliance in which a decrease of the upward y vertical limb stiffness enabled the leg to move upwards more freely. The virtual compliance methods slightly increased variability along the limb's planned pathway, but the anisotropic compliance control improved the successful negotiation of step obstacles by over 70% compared to isotropic compliance and positional control methods. We confirmed these findings in simulation and using a self-propelling bipedal robot walking along a linear rail over bumpy terrain. While the importance of limb compliance for stance interactions have been known, our results highlight how limb compliance in the swing-phase can enhance walking performance in naturalistic environments.

1. Introduction

The natural world challenges walking in animals and robots. Large structures within the environment prompt navigational planning [1] while smaller substrate irregularities disrupt limb motion and foot placement [2]. These smaller irregularities impact both stance and swing phases of walking. During the stance phase the limb is in contact with the ground and substrate unevenness may induce body instability. Substantial effort has been devoted to improving robot stability through stance adaptations, including understanding how foot placement [3–5], force control [2, 6, 7], and traction control [8–10] improve walking over uneven ground. However, less focus has

been devoted to the influence of ground unevenness during the swing phase as the limb is lifted and moved forward to the next stance location [11]. In cluttered environments swing motions of the leg may cause collisions with surrounding obstacles that destabilize walking (figure 1) or damage the limb. In this paper we present a method for controlling the swing phase of a robotic leg that incorporates limb compliance to enable effective interaction with obstacles.

In principle, control of swing phase should be simpler than that of stance phase. During stance, the limbs produce ground reaction forces to support and propel the body while adjusting for instabilities and preventing slipping. In contrast, during swing the limb simply moves through the air to reset for the



next stance. This perspective is reinforced by observations of running animals in which the stance duration shifts with speed or when substrate roughness changes, whereas swing duration is mostly conserved [12–14]. However, experimental findings show that limb swinging is metabolically costly [15], and swing-leg kinematic adjustments are employed to compensate for body perturbations [16, 17]. Experiments on running guinea fowl over uneven surfaces indicate that limb muscles actively prepare the limb during swing prior to stepping on an obstacle [18]. Modeling of human walking shows that limb compliance improves recovery from swing-phase perturbations, extending successful negotiation of ground discontinuities from 3.5% of limb length to 35% [19]. Natural terrain is rarely flat, suggesting that swing perturbations may occur frequently. This is especially important for smaller animals and robots, which experience relatively more complex ground terrain [20] and use higher stride frequencies that limit sensory and recovery processing time. Observation of ants walking on an artificially bumpy substrate revealed that the swing-phase of up to 11% of strides was disrupted by a limb-ground collision outside of the preferred stance location [21]. Recovery from perturbations during walking likely occurs frequently in natural environments, with limb control during swing phase contributing to stability and recovery.

The importance of compliance for controlling the forces that robots and animals impart on the world has been known for many years. For example, Neville Hogan introduced the concept of ‘impedance control’ for robot arms where a control system

modulates the torques of the motors to emulate a spring-mass-damper system [22]. By emulating compliant behavior robots were able to interact with unexpected obstacles in a stable, and safe manner, without the need to re-program motion trajectories. Similar principles are thought to apply to humans, for example the stiffness of the human arm is modulated and tuned for effective interactions with objects [23, 24]. In a particularly convincing example, Hogan demonstrated that an impedance controlled robot arm can be commanded to move through a rigid obstacle and the arm does not suffer any instability because the robot-obstacle interaction is accommodated by the virtual stiffness of the controller [25]. We take a similar approach in this paper, commanding a leg to move in the swing-phase through an interfering rigid obstacle to study how the control method influences leg swing success.

Previous work on swing-limb control in robotics typically falls into one of three categories: (1) tactile, force, or inertial sensors on the legs and feet to detect collisions and re-plan trajectories [26–29], (2) visual trajectory planning to avoid obstacle collisions [30–33], or (3) feedforward swing trajectories tailored to different substrates or locomotion modes [2, 34, 35]. In most implementations of swing motion the limb is controlled through position control and thus requires active adjustment to the swing-phase trajectory when obstacles are encountered. However, inspired by the neuromuscular control of human limb compliance in both legs [17, 19, 36] and arms [23, 24], we seek to explore how compliance may enable robot legs to successfully negotiate obstacle-leg collisions during the swing-phase.

Limb compliance can be implemented through combinations of two mechanisms: (1) passive compliance by incorporating spring and damper elements directly into the mechanical structure of the limb, or (2) virtual compliance control in which a control system of actuators and sensors actively replicates the spring-damper behavior of compliant limbs. Direct incorporation of compliance elements into legged robots have been explored extensively through series-elastic actuators [37, 38], series and parallel springs [39–43], and distributed compliance in soft robotics [44, 45]. These methods provide passive compliance properties directly to the limb for fast, predictable, and energy efficient behavior [46]. However, with a few exceptions [42, 47], passive mechanical compliance elements are typically not reconfigurable and thus the limb stiffness cannot be modulated in real-time. Virtual compliance methods are implemented through feedback control of motor torque and measurements from appropriate sensors to make the limb emulate a compliant behavior [48, 49]. This behavior can be implemented by direct measurement of ground interaction forces through a force sensor at the foot [50], or by proprioceptive measurements such as measuring joint angles within the actuators [48, 49, 51]. Critically, proprioceptive-based methods rely on actuator and transmission systems that have low gear-ratios, low friction, and high backdrivability [52, 53]. Direct-drive actuation achieves all of these qualities and is increasingly prevalent in the regime of medium-small legged robots [39, 54–59]. The low-gear ratio motors provide tight control over the forces that legs impart on the ground enabling impressive dynamic robots [60]. These robots also share many common features which include: (1) direct or quasi-direct drive actuation, (2) parallel linkage legs for reduced inertia, and (3) high-torque density brushless DC (BLDC) motors. A comprehensive review of direct-drive legs with application to proprioception and force control can be found in [53]. This class of robots presents an optimal system for studying swing-phase compliance because then we can evaluate leg–obstacle interactions that occur along the entire leg without needing specific tactile force sensors to localize the contact.

In this paper we present the design of a simple direct-drive robot leg capable of dynamic movement and control. We study the performance of this robot walking over a step obstacle and on uneven substrate, subject to swing-phase collisions. In particular we compare three methods of swing-phase control: (1) position control, (2) compliance control independent to the direction of deflection, and (3) compliance control dependent on the direction of deflection with deflections in the upward direction having a lower virtual stiffness of the limb. We hypothesize that mode 3 will perform the best in leg–obstacle

collisions as it enables the leg to collide with obstructions and accommodate these collisions through passive leg movement up and over the obstacle. We will demonstrate that this method of anisotropic compliance control improves obstacle-leg interactions during swing without the need for trajectory re-planning or tactile sensing. Thus we propose that it may be useful in situations where leg movements are fast and the environment is complex. With passive leg compliance, legged robots can achieve improved obstacle-overcoming capabilities reducing the need for computationally costly sensors or sophisticated rerouting algorithms.

2. Methods

2.1. Leg design and control

To study swing-phase performance in the presence of obstacles we developed an experimental walking robot platform (figure 2(a)). Two robot legs were mounted to a linear bearing system that allowed for free walking along forward–backward direction while constraining motion in the vertical and lateral directions. Motor controllers, motors, and encoders were mounted on the moving stage. Each leg consisted of a 5 bar planar linkage system with links fabricated from a 1.22 cm thick aluminum. The link lengths were inspired by [61] and dimensions listed in figure 2. Leg links were joined at rotational joints with deep groove ball bearings ($10 \times 22 \times 6$ mm).

Each leg was controlled by two BLDC motors that actuated the legs as seen in figure 2. These low-profile outrunner motors (Quantom 5250, DYS motors) are common in recent small to mid-size legged robots [54–59]. Motor current control for the two motors were performed by a single ODrive motor controller (ODrive Robotics, Richmond, CA), which performed commutation at 10 kHz. Additionally, the ODrive provided closed-loop PID position control and closed-loop current control through commands from an external computer. Motor position was measured by capacitive rotary encoders mounted on the motor base (AMT-CUI 102). Each encoder provided quadrature signals with a step-resolution of 8192 counts per revolution. The robot was mounted on linear rails (SBR20-2200 mm) with linear bearings (SBR20-20 mm) providing low friction translation along the fore-aft direction. A summary of geometry and actuation components can be found in table 1.

Trajectory generation and control was performed on a computer with either position or current commands sent to each ODrive at 100 Hz over USB serial port. While 100 Hz is relatively slow for closed-loop limb control, our experiments focused on low-speed swing movements (0.5, 1, and 2 s swing duration) where this rate was sufficient. We executed all trajectory generation and control in Python using NumPy [62] and SciPy libraries [63].

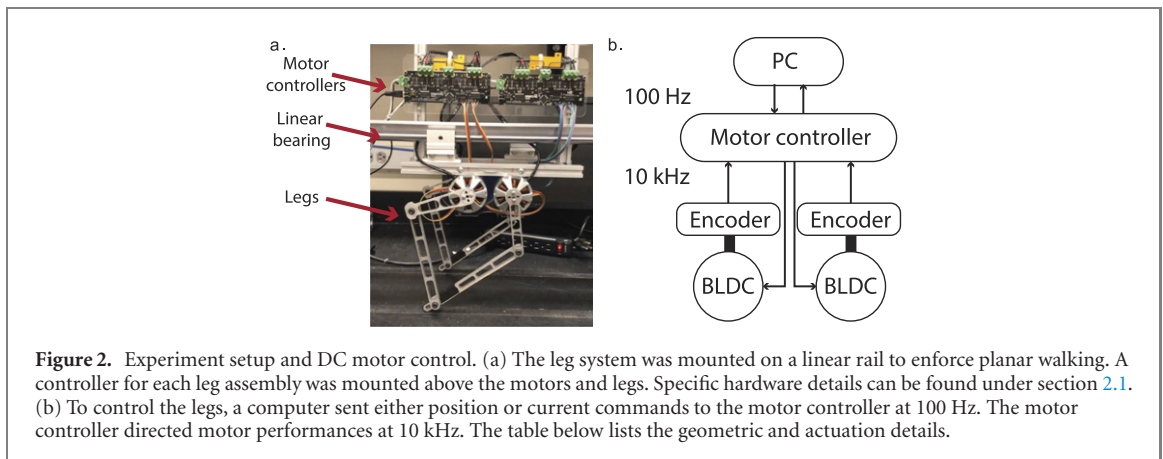


Table 1. Table of geometric and actuation parameters for the experiment.

Name	Detail
l_1	9 cm
l_2	16 cm
w	7 cm
Motors	Quantum 5250
Encoders	CUI AMT 102
Motor controller	ODrive

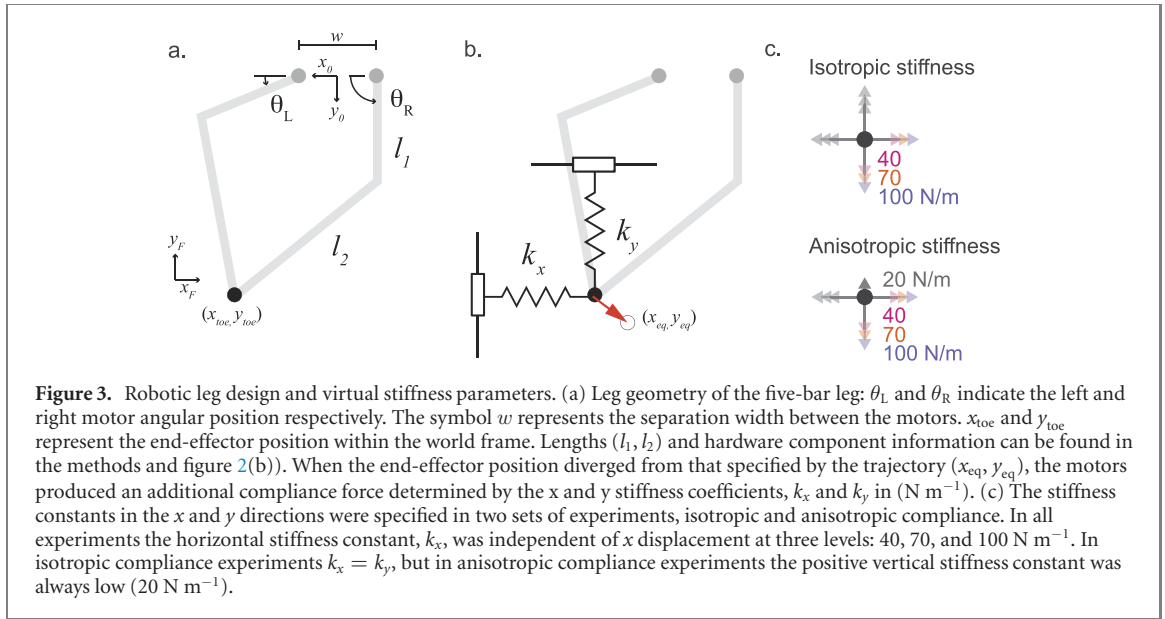
The signal control pathway from the computer varied for our three control methods: (1) position control, (2) isotropic stiffness, (3) anisotropic stiffness. In position control, angular position commands were directly sent from the computer to the ODrive which performed high-gain proportional–integral position control on each motor in the motor’s coordinate system. In the isotropic and anisotropic stiffness conditions, we calculated the instantaneous position of the leg’s toe using forward kinematics, and then calculated the error between toe location and desired location. The motor torques associated with the toe error and the virtual compliance were then calculated using the Jacobian of the leg in its current configuration and the required motor currents were sent to the ODrive during each control loop.

2.2. Virtual compliance implementation

Virtual compliance in robotic appendages usually involves modeling the dynamic response of either joints (joint-space) or the end-effector (task-space) as if governed by spring-mass-damper dynamics. The dynamics are implemented in a control system, rather than using physical devices such as torsion springs, and thus this approach has been called virtual compliance control in the legged robotics literature [49, 51]. Implementation of the full spring-mass-damper dynamics requires continuous integration of the dynamics equation to determine the appropriate joint torques. However, many implementations have focused on emulation of just the spring, or spring-damper dynamics, which only require position and velocity to determine [64].

In this work we developed a compliance controller by emulating a virtual spring in the toe coordinate system of a two degree-of-freedom planar robot leg (figure 3). We implemented this virtual spring with varying magnitudes of spring stiffness in the x and y directions in either isotropic or anisotropic configurations (figure 3(c)). In the isotropic configuration the y stiffness was the same whether the toe was displaced above or below the set point. However, in the anisotropic configuration the y stiffness was lower when the toe was displaced vertically above the setpoint (figure 3(c)). We hypothesized that this anisotropy would enable effective obstacle foot interaction during swing trajectories since the foot could move with less resistance in the direction of low stiffness (upwards), and thus could be pushed up and over obstacles during swing.

The simple compliance controller we developed for our leg used the quasi-static force–torque relationship, $\tau = J^T F_{\text{toe}}$, where J is the Jacobian of the leg. The compliance controller was evaluated in a control loop running at 100 Hz. We defined the setpoint position of the foot, $[x_{\text{eq}}, y_{\text{eq}}]^T$, as a parabolic trajectory with maximum height in the middle of the swing phase. We then calculated the horizontal position error, $\Delta x = (x_{\text{toe}} - x_{\text{eq}})$, and the vertical position error, $\Delta y = (y_{\text{toe}} - y_{\text{eq}})$. We defined the positive x direction in the direction of the forward swing trajectory (x_F , figure 3(a)) and the positive y direction away from the ground, (y_F , figure 3(a)). The motor torque to implement this virtual force was given by the following relationship between toe position and



motor torques

$$\begin{bmatrix} \tau_1 \\ \tau_2 \end{bmatrix} = -J(\theta_L, \theta_R)^T \begin{bmatrix} k_x & 0 \\ 0 & k_y \end{bmatrix} \begin{bmatrix} \Delta x \\ \Delta y \end{bmatrix}. \quad (1)$$

Isotropic stiffness control simply relies on evaluation of equation (1) with constant values for k_x and k_y (figure 3(c)). However, in anisotropic stiffness control we provided different values for k_y depending on whether the foot was displaced above the setpoint ($\Delta y > 0$) or below the setpoint ($\Delta y < 0$). Anisotropic stiffness was only examined for the vertical axis and not the horizontal axis since we wanted to ensure good trajectory tracking in the fore-aft direction. We chose a lower stiffness value for upwards displacements of the foot so that foot–obstacle interactions would tend to push the leg up and over the obstacle (figure 3(c)). We chose three magnitudes for the isotropic stiffness constants $k_x, k_y = [40, 70, 100]$ N m^{-1} . In anisotropic compliance mode, we reduced the positive vertical stiffness constant to 20 N m^{-1} , allowing the leg to more freely deviate from the swing trajectory in the positive vertical direction (away from the ground). In all other directions the stiffness was constant and held at one of three values, $k_x, k_y = [40, 70, 100]$ N m^{-1} . We determined this stiffness range by balancing: (1) if stiffness is too low other un-modeled effects such as bearing friction will cause the behavior to deviate from the desired stiffness, and (2) if stiffness is too high then small displacements from the setpoint will cause the motors to reach their maximum torque output and thus the leg behavior will deviate from the desired stiffness profile. We calculated the required motor torque for stiffness control across the entire workspace of the robot leg and evaluated at what values of k_x , and k_y the motor torque would reach maximum (see SI (<https://stacks.iop.org/BB/16/056001/mmedia>) figure 1). We found that stiffness values of above

$\approx 100 \text{ N m}^{-1}$ lead to motor saturation for displacements of half a stride length, equivalent to a leg colliding at mid-swing (see SI figure 2). Thus the chosen stiffness range reflects the maximum motor torque of the actuators in this experiment and a similar calculation would have to be performed to determine an appropriate stiffness range for other robots.

Lastly, gravity prevented the end-effector from reaching equilibrium locations with nonzero vertical positions. Therefore, in all experiments we compensated for the gravitational moments on the links through a joint-angle dependent feed-forward current added to the control signal. The gravity compensation throughout the swing motion was generated from measurements of the current needed to maintain the leg's position at various locations in the workplace.

2.3. Experimental procedures

2.3.1. Compliance validation

To test the validity of our compliance control we performed static measurements of vertical stiffness. We applied downward vertical forces by hanging masses at the toe joint and measured the resulting vertical deflection of the toe. We measured the stiffness of the robotic leg by fitting the force versus displacement relationship with the function $F = k_y \Delta y$. Compliance validation was performed for the full gravity compensation algorithm described above and thus only depended on applied load. We measured vertical stiffness from an initial configuration with the toe directly centered between the motors in x direction, and at a height of 4 cm in the y direction.

2.3.2. Body-fixed swing-phase collision recovery

We performed systematic obstacle-collision experiments to determine how leg compliance affects collision recovery during the swing phase (figure 4). We

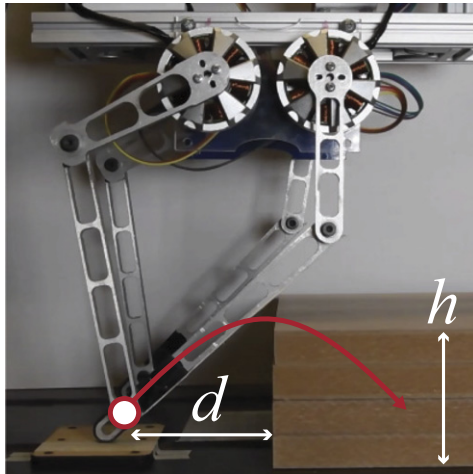


Figure 4. Stationary step obstacle experiment set-up. The robot chassis is fixed in place and a single leg is commanded to follow a parabolic swing trajectory with an obstructing step obstacle of height, h , and distance from mid-swing, d . Picture shows obstacle configuration with $d = 50\%$, and $h = 5.6$ cm.

used the same swing trajectory for all experiments, a parabolic motion that reached 4 cm vertical height at mid-swing, and had a total swing length of 18 cm in the forward direction and centered longitudinally on the middle of the robot. The obstacles in these experiments consisted of stacks of smooth MDF particle board, each 1.9 cm tall. Particle board was stacked to a desired height and distance and was presented to the leg as a flush vertical step (i.e. if multiple MDF layers were used they were all aligned so that the step had a smooth vertical face). Accounting for the length of the toe, the step heights tested were $h = [1.8, 3.7, 5.6]$ cm above the toe joint during stance, set at a distance d from the starting swing location. The step distance was measured as a percentage of the forward swing length, with mid-swing occurring at $d = 50\%$. We performed step experiments over the range, $d = [20\%, 30\%, 35\%, 40\%, 45\%, 50\%, 55\%, 60\%]$. We did not include test combinations in which the toe swing trajectory would not interact with the step. To maintain a quasi-static relationship, the body-fixed swing trajectory was kept constant across all experiments using a swing duration of 2 s. For all combinations of step location, step height, and control type we performed 25 trials. We defined a successful swing phase as one where the foot completes a swing ending with the foot fully on top of the step. Unsuccessful swing phase movements occurred when the leg hit the obstacle and was not able to make it to the top of the step (see supplementary video).

2.3.3. Free walking with swing-phase obstacle collisions

We expanded experiments to more naturalistic conditions using a vertically supported bipedal system to walk over uneven terrain (figure 5). We mounted

the robot chassis to a linear bearing enabling the system to slide freely along the dual bearing shafts in the forward direction while being supported in the vertical direction. The substrate was constructed from 3 pieces of mortar block (144 cm long total) with rough rocks of varying heights placed at random locations. We also scattered gravel among the rocks. The embedded rocks had an average height of 3.1 cm with a maximum height of 5.6 cm (figure 5(c)).

The robot was programmed to walk with a stride length of 10 cm, capable of traversing the 144 cm long trackway within 15 strides. We programmed the robot to walk using six swing phase heights (1.5, 2.0, 2.5, 3.0, 3.5, and 4.0 cm) and the two compliance control methods. In each trial, the robot was allowed to complete 15 strides before measuring the forward distance traveled by the left toe. The robot started from a consistent initial position in each trial, therefore interacting with the same embedded rocks.

We tested isotropic and anisotropic compliance control methods but we did not test forward walking with position control which performed poorly in the stationary step obstacle experiment. Under isotropic control, x and y stiffness values were set to 150 N m^{-1} . This stiffness was higher than those tested during the stationary step obstacle experiment in order to generate appropriate ground-reaction forces for the stance foot. Under anisotropic conditions, the y stiffness in the upwards vertical direction was reduced to 15 N m^{-1} , allowing for higher vertical deviations of the foot. Both isotropic and anisotropic control modes used identical stance trajectories to produce similar ground reaction forces. All performance differences between control methods occurred during swing.

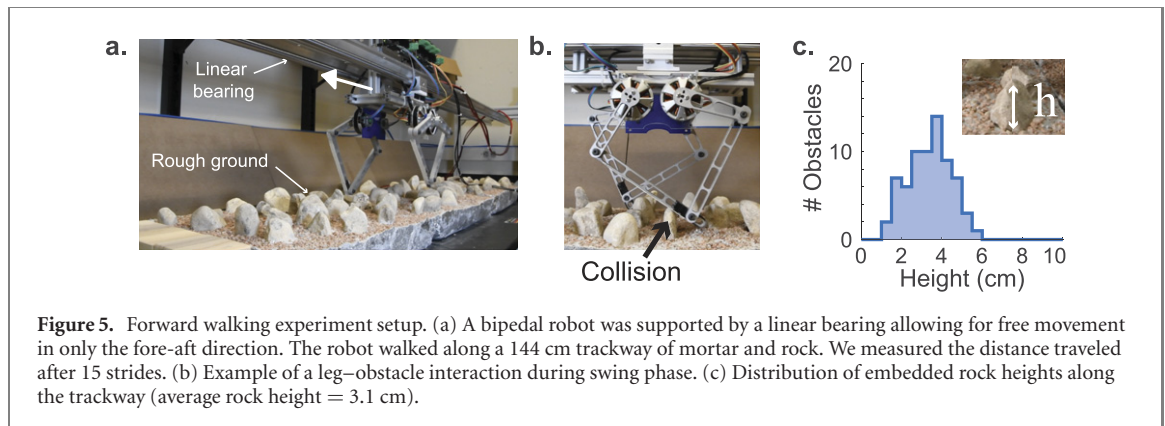
2.4. Simulation

We performed simulations of the body-fixed experiments using the Simulink Simscape multibody physics package (MATLAB, Natick, MA) to simulate rigid-body kinematics. We programmed a PI position controller to model the ODrive position control with torque saturation at the maximum torque value of the motor. The compliance control was implemented using the same algorithm described in methods in which we solved for the torques in equation (1) at each time-step of the simulation. Contact was modeled using a spring-damper contact model and was handled by the Simulink Simscape contact forces package.

3. Results and discussion

3.1. Stiffness measurement

We first compared the difference between the specified and experimentally measured leg stiffness. We measured the vertical stiffness of the stationary limb under each compliance level. Consistent with a linear spring-stiffness, vertical deflection of the toe increased approximately linearly with applied



force (figure 6(b)). For the specified conditions of $k_y = [40, 70, 100] \text{ N m}^{-1}$, we calculated an actual stiffness of $k_y = [31.5 \pm 9.0, 59.5 \pm 7.8, 98.2 \pm 11.2] \text{ N m}^{-1}$ respectively.

Simulations of the same stiffness experiments were able to exactly reproduce the specified virtual stiffness values. The simulated stiffness response and commanded stiffness were identical (open-circle simulation results overlap with the commanded stiffness shown as transparent line; figure 6(d)). The simulation results suggest that the deviation in experiment at lower stiffness is due to unmodeled phenomena such as bearing friction or motor cogging. While the joints of the legs had roller bearings to reduce friction, there was still a small amount of resistance in the system. Similarly, cogging torque results from magnetic interactions within the motor that produce a small resisting torque opposing motion. At low motor stiffness values, the resistance due to bearing friction and cogging torque may be more appreciable because the commanded motor torques are lower. However, at higher stiffness the relative influence is reduced or negligible.

3.2. Swing trajectory tracking with no obstacles

We next sought to determine the swing trajectory tracking performance for the three control methods without obstacles. We compared the tracking performance for the toe to follow a parabolic swing trajectory for each control mode (positional, isotropic compliance, and anisotropic compliance) using three swing durations (0.5, 1, and 2 s) in which the toe was commanded to move at constant velocity through the swing motion (figure 7).

The position control demonstrated the most accurate tracking in experiments, especially for longer swing durations (bottom row, figure 7). Isotropic and anisotropic compliance control tracked the first half of swing within a few millimeters but deviated more strongly towards the end of swing. The deviation from the specified trajectory was worst for the low stiffness (40 N m^{-1}) and faster speeds (0.5 s duration) swing motions. The anisotropic control showed the worst tracking with the toe location consistently rising above the commanded swing trajectory. This

overshoot in the vertical direction is expected from the relatively low stiffness (20 N m^{-1}) in the positive vertical direction, combined with the larger vertical momentum of the leg during the first half of the swing trajectory.

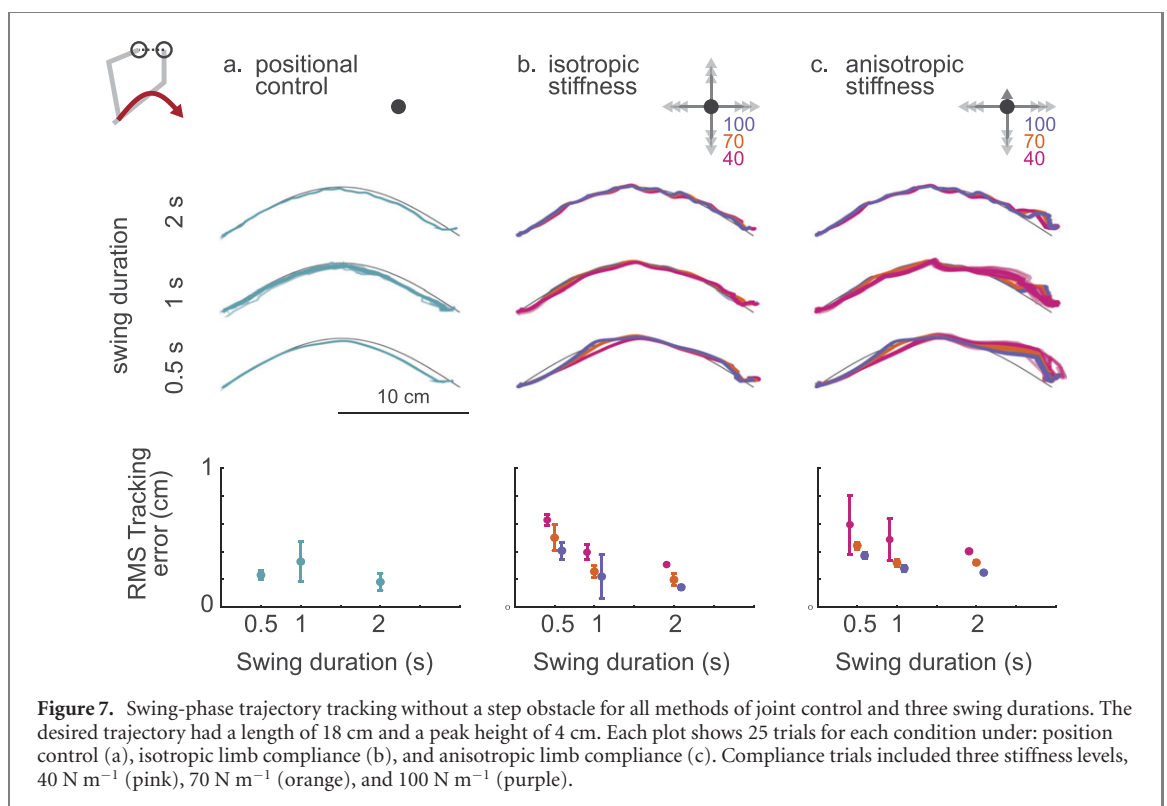
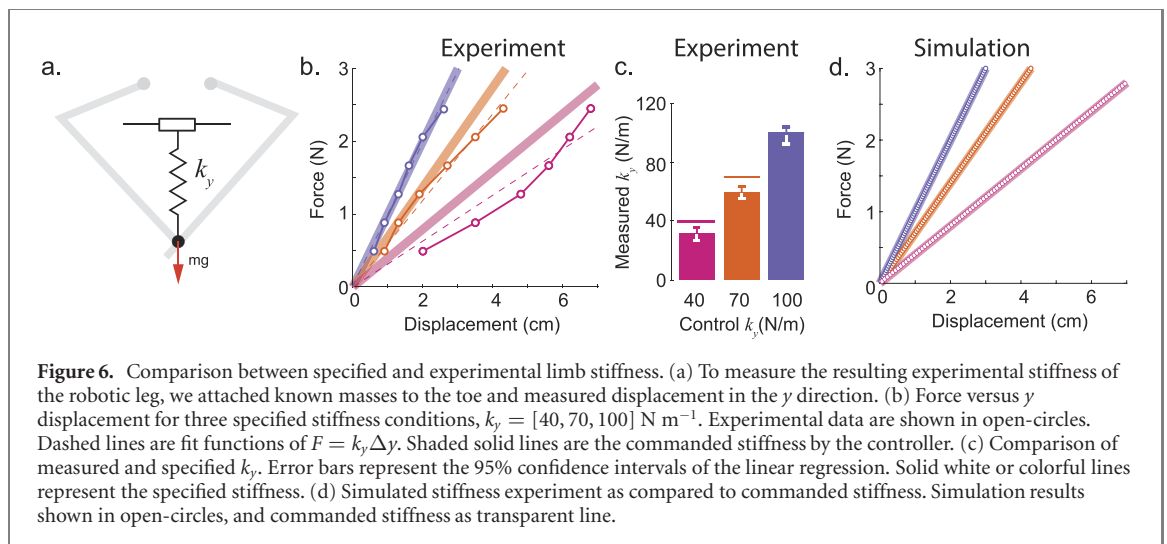
3.3. Foot–obstacle interaction in fixed body experiments

3.3.1. Position control

To test position control of the motors, the motor angles were directly specified during the swing phase to track the parabolic swing trajectory. In experiments with position control, the leg failed to reach the top of the step in all but the shortest step height, $h = 1.8 \text{ cm}$ (figure 8). With taller steps, the lower-link of the leg consistently hit the edge of the step and became stuck (figure 9, top row). Averaging across all step height and step distance experiments (13 conditions of 25 trials each), position control of the leg enabled successful recovery of swing motion after colliding with the step in less than 10% of the experimental trials (figure 8(b)).

Our results indicate that position control of the leg joints is highly problematic for swing phase collisions. As the limb collides with the step the foot is displaced above the swing trajectory, resulting in the motors attempting to push the foot downward. Consequently, the foot becomes jammed against the obstacle, unable to reach the top of the step (figure 9(a)). This increase in leg–obstacle force can be clearly seen in the simulation results (figures 9(b)–(e)). When the leg collides with the obstacle the simulated position controller continues to increase motor torque because the joint tracking error becomes large, this manifests as a larger contact force between the leg and obstacle ultimately jamming the leg in place.

Although recovery from a swing phase collision using direct motor position control can be robust, it requires both collision detection and trajectory re-planning. One strategy involves re-targeting of the limb around the obstacle, as has been investigated in previous studies [28, 65, 66]. An alternative strategy for recovering from a swing collision involves retracting the foot to the highest possible swing phase



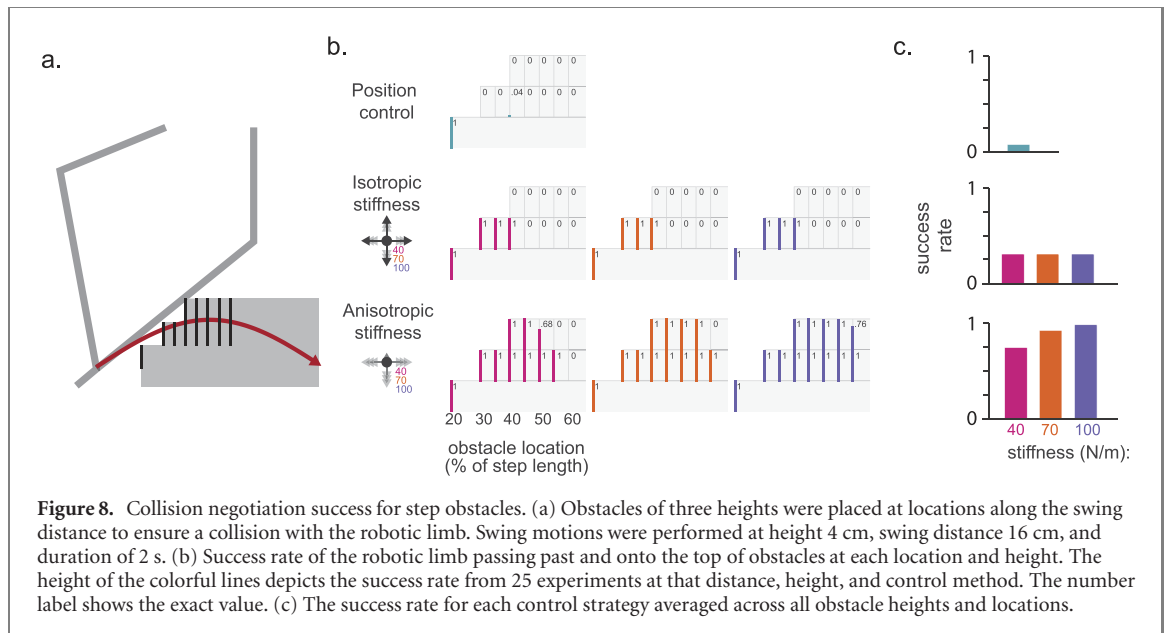
trajectory after detecting a collision. However, this high-swing tactic increases energy usage, decreases body stability, and requires either a longer swing duration or faster swing speeds compared to lower re-targeting strategy. Both of these strategies require active sensing for collisions, while the compliance control methods we next describe do not require modulation of control gains or re-planning to accommodate leg–obstacle interactions.

3.3.2. Isotropic compliance control

Under isotropic compliance control the virtual stiffness was equal in the horizontal and vertical directions. Our experimental results demonstrated that isotropic compliance control improved the overall

swing performance of the leg across all the step conditions (figure 8). The leg demonstrated 100% success for steps less than the programmed swing height (4 cm) and a distance of 40% the stride length (figure 8). However, when the step was placed further from the start of the swing trajectory or with higher steps, the isotropic stiffness control failed every time in experiments (uncolored squares, figure 8).

Equal compliance in the horizontal and vertical directions did not improve swing collision recovery during the second half of swing or for tall obstacles. Due to the geometry of the leg linkages, most collisions occur along the lower link which we call the ‘shin’. When the shin collides with an obstacle in the first half of the swing motion the trajectory of the



toe is moving in the positive vertical direction which enables the shin to slide along the step edge with the foot passing onto the step. However, with step heights above the swing trajectory height or at step locations $>50\%$ through the stride, the toe is following a downward trajectory which results in the shin actively pushing into the step and causing failure similar to the position control method. The overall success of the isotropic compliance control in experiment was not influenced by the stiffness value over the range we examined (figure 8(c)).

3.3.3. Anisotropic stiffness control

We implemented anisotropic stiffness control in which the horizontal and downward stiffness values were equal at 40, 70, or 100 N m^{-1} and the upward stiffness was lower, at a value of 20 N m^{-1} . Across all three stiffness levels, the limb successfully advanced past the step obstacle to the top of the step in over 75% of the experimental tests. Collision recovery improved with increasing stiffness, reaching a $>98\%$ success rate at 100 N m^{-1} (figure 8(c)).

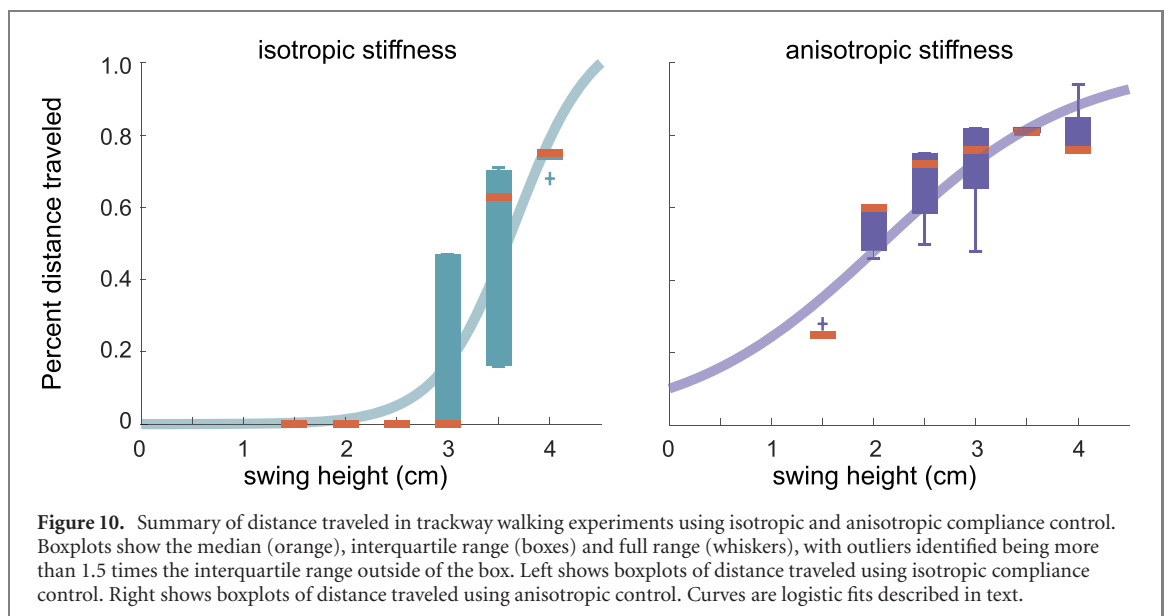
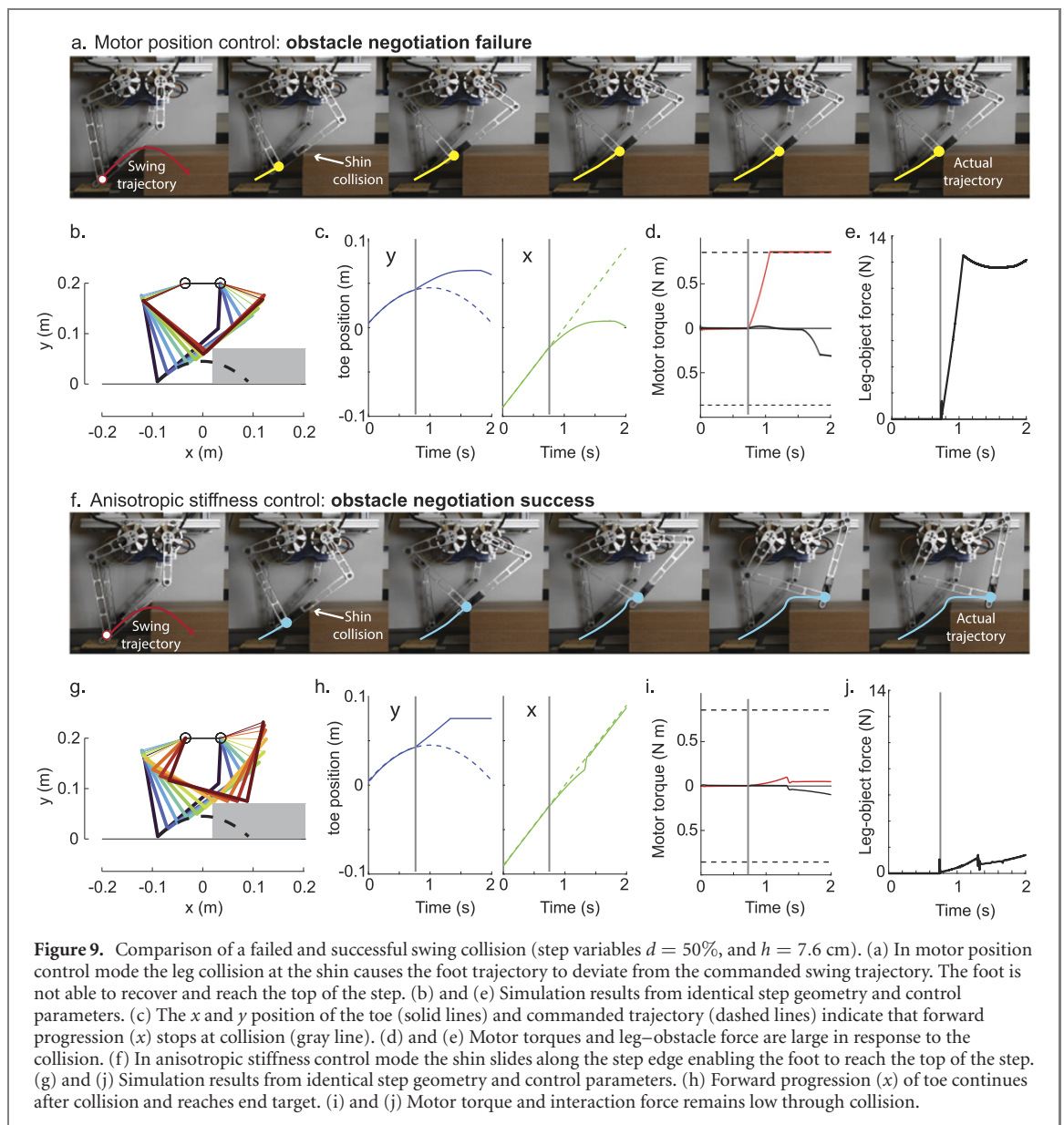
The improved collision recovery observed under anisotropic compliance control in experiments is likely due to the geometry of the limb and deflection pattern at collision. As the shin collides with the step obstacle, the limb is pushed backward and upward. Since the stiffness is lowest in the upward direction, the collision causes the linkages in the leg to fold, bringing the toe further away from the ground and towards the top of the step (9, bottom row). The high horizontal stiffness ensures that the leg continues to advance forward, causing the shin to slide along the step edge. Simulation of the anisotropic compliance demonstrate how low upwards ‘stiffness’ keeps the leg–obstacle contact force low while the leg slides upwards and across the step (figure 9(j)). The commanded motor torques during the obstacle

interaction are low as well and thus anisotropic compliance may be favorable from an energetic or torque-limited perspective. Anisotropic conditions with a higher horizontal stiffness perform better by allowing a larger upward y deflection while keeping the horizontal deflection low, thus pushing the toe up onto the step (figure 8(c)).

Anisotropic stiffness improved swing collision recovery, but demonstrated a trade-off with trajectory accuracy. Allowing the limb to deflect up and away from obstacles with low resistance and improving swing performance. However, the anisotropic vertical stiffness also resulted in trajectory deviations due to link inertia. To resolve this issue the control calculations could explicitly account for link inertia and Coriolis forces, producing a more complex but more comprehensive model of the limb dynamics. Even while using a relatively simple controller, anisotropic stiffness control provided a robust method for limbs to passively deflect past swing-phase collisions.

3.4. Swing-phase collisions with rocks during forward walking

For the forward walking experiment, the isotropic swing control failed to move even a single step forward when the step height was below 3 cm (figure 10). The forward travel distance increased as the step height increased. When the step height was close to the average object height the isotropic control enabled a traversal distance of 73% of the total trackway length. The failure in the isotropic control experiments were caused by limb jamming due to swing collisions with embedded rocks. The robot would rock back and forth with no net displacement due to the jammed limb. This limb jamming was particularly common when the limb collided during the second half of swing phase. Similar to observations during the stationary step obstacle experiments,



collisions during the second half of swing pushed the limb downward preventing the toe from sliding above the obstacle. However, different from the fixed base experiments these collisions during the second half of swing caused the robot chassis to be pushed backwards, thus leading to no forward progression and repeated interactions with the same obstacle.

Under anisotropic control the robot traveled further for each of the swing heights when compared to the isotropic control. To statistically compare these two experiments we fit a logistic regression to the isotropic and anisotropic travel distance, $y = \frac{1}{1 + \exp(-\alpha(x - h_0))}$, where α governs the slope of the curve and h_0 is the location where the success rate exceeds 50%. We found that the success rate exceeded 50% for isotropic compliance at a height of $h_0 = 3.5 \pm 0.1$ cm, while for the anisotropic compliance the success rate exceeded 50% at $h_0 = 2.0 \pm 0.1$ cm. The uncertainty estimates on h_0 are generated from the nonlinear least squares fitting routine in Matlab and are 95% confidence intervals. The anisotropic compliance control significantly improved the walking performance when the step height (compared to obstacle height) was low.

4. Conclusions

We find that limbs with a low upward vertical stiffness recover from swing-phase collisions, improving robotic walking over uneven ground. Previously, limb compliance has been beneficially applied during the stance phase of robot walking to control the ground reaction forces on uneven terrains [2, 67]. Here, we demonstrate that otherwise impassable swing-phase collisions do not impede direct-drive robotic limbs when incorporating a relatively rudimentary stiffness control method. Uniform ('isotropic') stiffness in the horizontal and vertical directions provided only some improvement in swing obstacle negotiation, however, the application of anisotropic limb compliance increased the success rate of continuing past a swing collision from 5% to 98% compared to positional control. By implementing anisotropic stiffness using a high relative stiffness in all directions except for vertically away from the ground, the toe deflects upwards and onto the top of step obstacles. The improved recovery from swing obstacles was confirmed in a walking bipedal robot. Walking trials that used an anisotropic compliant control strategy traveled longer distances over uneven terrain, including enabling forward progression under several conditions that completely halted the robot when using limbs with equal, isotropic stiffness in all directions. Our stiffness control used a simplified approach, assuming that leg motion is slow and quasi-steady, therefore ignoring dynamic effects in the limb motion. However, this approach could be generalized to faster movements or different morphologies by incorporating the dynamical components into the impedance model [22].

Our finding that compliant limbs improve collision recovery in a robot has also been observed during insect walking. While the size-scale and the dynamics of insects differs from that of our larger, heavier robot, the observation that limb compliance improves swing perturbation recovery demonstrates its importance for systems that navigate unstructured environments. The limbs of cockroaches contain elastic materials [68] that enable them to bend and flex passively in response to external perturbations [69]. When subjected to an impulse perturbation, cockroach limbs return to their original position within 40 ms [70], opposing the disturbance faster than possible through active control. Since small animals, including cockroaches, navigate relatively rough terrain [20] and run with a high stride rate, passive perturbation recovery due to elastic structures in the limbs likely occurs often under real-world circumstances.

While recovery from limb collisions during swing has been directly studied in only a few species, many animals possess anatomical structures that prescribe joint range of motion and limb compliance. For example, bone and cartilage structures in the knee correspond to walking posture and biomechanics in mammals [71, 72]. Generally, limb compliance in vertebrates is primarily determined by connective tissue, including muscles, tendons, and ligaments [73, 74], however bone bending can also contribute, sometimes to an extreme, as in bat wing bones [75]. In invertebrates, limb stiffness depends on both exoskeleton composition and three-dimensional structure. The exoskeleton cuticle often comprises relatively stiff chitin fibers and rubber-like resilin proteins, though water content and sclerotization (hardening) impact the material properties of each [76]. The structure and ordering of joints within the limbs also govern the deformations and anisotropy of limbs during walking [77]. Further, some studies have directly observed the directionality of limb structures during legged locomotion. For example, spiders and cockroaches running across wire-mesh orient their limbs vertically to catch wires with tarsal spines, which then collapse during limb withdrawal preventing interference [78]. Ants jam their limbs and antennae against tunnel walls to decelerate vertical falls, aligning these appendages vertically along the tunnel axis [79]. Given that animals possess numerous potential sources of stiffness within their limbs, compliance likely impacts walking performance including during swing perturbation recovery and influenced by the directionality of limb movements.

Unlike biological limbs, our direct-drive robotic limbs do not include elastic materials and instead use a virtual compliance control system to emulate an elastic leg response. Virtual compliance methods are useful because they enable rapid modulation of stiffness without requiring mechanical reconfiguration. This potentially enables more complex models of limb

stiffness, such as the anisotropic stiffness studied here, to be easily implemented through virtual compliance while such a limb stiffness may be difficult to implement through mechanical design. While not investigated in this study, virtual compliance models present opportunities to examine dynamic stiffness control that varies throughout the swing phase. For example, the role of k_x is relatively unstudied in this work however there may be leg configurations where low k_x in the backward direction would enable a limb to move back and up over an obstacle. Future studies should explore how the axes of stiffness (principle components of the elasticity matrix) and the directions of anisotropy influence leg–obstacle interaction.

Critically, the anisotropic compliance control applied in this study improved recovery from swing phase perturbations without adding significant computational complexity. Our stiffness calculations used only motor feedback based on leg kinematics. Alternative approaches commonly applied in legged robots often require sensing a perturbation, shifting to a recovery program, and re-planning the limb trajectory. Robots that rely on these strategies require additional physical components (such as visual obstacle detectors or inertial measurement units) and incur higher computational costs. As a result, these robots are heavier, have increased external power requirements, and experience temporal latency when responding to perturbations. We anticipate that an anisotropic compliance model, like that presented in this study, present an effective complement for legged robotics, particularly those that operate at faster stride frequencies and traverse complex terrain.

Data availability statement

The data that support the findings of this study are available upon reasonable request from the authors.

ORCID iDs

Glenna Clifton  <https://orcid.org/0000-0002-5806-7254>

Nick Gravish  <https://orcid.org/0000-0002-9391-2476>

References

- [1] Chilian A and Hirschi Müller H 2009 Stereo camera based navigation of mobile robots on rough terrain *2009 IEEE/RSJ Int. Conf. on Intelligent Robots and Systems* (Piscataway, NJ: IEEE) pp 4571–6
- [2] Hodgins J K and Raibert M N 1991 Adjusting step length for rough terrain locomotion *IEEE Trans. Robot. Automat.* **7** 289–98
- [3] Koolen T et al 2012 Capturability-based analysis and control of legged locomotion, part 1: theory and application to three simple gait models *Int. J. Robot. Res.* **31** 1094–113
- [4] Zhao Y and Sentis L 2012 A three dimensional foot placement planner for locomotion in very rough terrains *2012 12th IEEE-RAS Int. Conf. on Humanoid Robots (Humanoids 2012)* pp 726–33 (ieeexplore.ieee.org)
- [5] Kuffner J, Nishiwaki K, Kagami S, Inaba M and Inoué H 2005 Motion planning for humanoid robots *Robotics Research. The Eleventh Int. Symp.* (Berlin: Springer) pp 365–74
- [6] Hauser K, Bretl T, Latombe J-C, Harada K and Wilcox B 2008 Motion planning for legged robots on varied terrain *Int. J. Robot. Res.* **27** 1325–49
- [7] Wensing P M, Wang A, Seok S, Otten D, Lang J and Kim S 2017 Proprioceptive actuator design in the MIT cheetah: impact mitigation and high-bandwidth physical interaction for dynamic legged robots *IEEE Trans. Robot.* **33** 509–22
- [8] Chopra S, Tolley M T and Gravish N 2020 Granular jamming feet enable improved foot–ground interactions for robot mobility on deformable ground *IEEE Robot. Autom. Lett.* **5** 3975–81
- [9] Hauser S, Eckert P, Tuleu A and Ijspeert A 2016 Friction and damping of a compliant foot based on granular jamming for legged robots *2016 6th IEEE Int. Conf. on Biomedical Robotics and Biomechanics (BioRob)* pp 1160–5
- [10] Ding L, Gao H, Deng Z, Song J, Liu Y, Liu G and Iagnemma K 2013 Foot–terrain interaction mechanics for legged robots: modeling and experimental validation *Int. J. Robot. Res.* **32** 1585–606
- [11] Desai R and Geyer H 2012 Robust swing leg placement under large disturbances *2012 IEEE Int. Conf. on Robotics and Biomimetics (ROBIO)* (Piscataway, NJ: IEEE)
- [12] Heglund N C, Taylor C R and McMahon T A 1974 Scaling stride frequency and gait to animal size: mice to horses *Science* **186** 1112–3
- [13] Pijnappels M, Bobbert M F and van Dieën J H 2001 Changes in walking pattern caused by the possibility of a tripping reaction *Gait Posture* **14** 11–8
- [14] Kuo A D 2001 A simple model of bipedal walking predicts the preferred speed–step length relationship *J. Biomech. Eng.* **123** 264–9
- [15] Marsh R L, Ellerby D J, Carr J A, Henry H T and Buchanan C I 2004 Partitioning the energetics of walking and running: swinging the limbs is expensive *Science* **303** 80–3
- [16] Desai R and Geyer H 2013 Muscle–reflex control of robust swing leg placement *2013 IEEE Int. Conf. on Robotics and Automation* (Piscataway, NJ: IEEE)
- [17] Song S, Desai R and Geyer H 2013 Integration of an adaptive swing control into a neuromuscular human walking model *Conf. Proc. IEEE Eng. Med. Biol. Soc.* vol 2013 pp 4915–8
- [18] Daley M A and Biewener A A 2006 Running over rough terrain reveals limb control for intrinsic stability *Proc. Natl Acad. Sci.* **103** 15681–6
- [19] Ernst M, Geyer H and Blickhan R 2012 Extension and customization of self-stability control in compliant legged systems *Bioinspir. Biomim.* **7** 046002
- [20] Kaspari M and Weiser M D 1999 The size–grain hypothesis and interspecific scaling in ants *Funct. Ecol.* **13** 530–8
- [21] Clifton G T, Holway D and Gravish N 2020 Uneven substrates constrain walking speed in ants through modulation of stride frequency more than stride length *R. Soc. Open Sci.* **7** 192068
- [22] Hogan N 1985 Impedance control: an approach to manipulation: Part I–theory *J. Dyn. Syst. Meas. Control* **107** 1–7
- [23] Kadiallah A, Liaw G, Kawato M, Franklin D W and Burdet E 2011 Impedance control is selectively tuned to multiple directions of movement *J. Neurophysiol.* **106** 2737–48
- [24] Gomi H and Kawato M 1996 Equilibrium–point control hypothesis examined by measured arm stiffness during multijoint movement *Science* **272** 117–20
- [25] Hogan N 1987 Stable execution of contact tasks using impedance control *Proc. 1987 IEEE Int. Conf. on Robotics and Automation* vol 4 pp 1047–54
- [26] Čížek P, Kubík J and Faigl J 2018 Online foot–strike detection using inertial measurements for multi-legged

- walking robots 2018 *IEEE/RSJ Int. Conf. on Intelligent Robots and Systems (IROS)* pp 7622–7
- [27] Pearson K G and Franklin R 1984 Characteristics of leg movements and patterns of coordination in locusts walking on rough terrain *Int. J. Robot. Res.* **3** 101–12
- [28] Ishikawa T, Kojio Y, Kojima K, Nozawa S, Kakiuchi Y, Okada K and Inaba M 2017 Bipedal walking control against swing foot collision using swing foot trajectory regeneration and impact mitigation 2017 *IEEE/RSJ Int. Conf. on Intelligent Robots and Systems (IROS)* pp 4531–7
- [29] Zucker M, Ratliff N, Stolle M, Chestnutt J, Bagnell J A, Atkeson C G and Kuffner J 2011 Optimization and learning for rough terrain legged locomotion *Int. J. Robot. Res.* **30** 175–91
- [30] Kanoulas D and Vona M 2014 Bio-inspired rough terrain contact patch perception 2014 *IEEE Int. Conf. on Robotics and Automation (ICRA)* pp 1719–24 (ieeexplore.ieee.org)
- [31] Albert A, Suppa M and Gerth W 2001 Detection of stair dimensions for the path planning of a bipedal robot 2001 *IEEE/ASME Int. Conf. on Advanced Intelligent Mechatronics. Proc. (Cat. No. 01TH8556)* vol 2 pp 1291–6
- [32] Chilian A and Hirschmüller H 2009 Stereo camera based navigation of mobile robots on rough terrain 2009 *IEEE/RSJ Int. Conf. on Intelligent Robots and Systems* pp 4571–6 (ieeexplore.ieee.org)
- [33] Okada K, Ogura T, Haneda A and Inaba M 2005 Autonomous 3D walking system for a humanoid robot based on visual step recognition and 3D foot step planner *Proc. of the 2005 IEEE Int. Conf. on Robotics and Automation* pp 623–8 (ieeexplore.ieee.org)
- [34] Arslan Ö and Saranlı U 2012 Reactive planning and control of planar spring-mass running on rough terrain *IEEE Trans. Robot.* **28** 567–79
- [35] Seyfarth A, Geyer H and Herr H 2003 Swing-leg retraction: a simple control model for stable running *J. Exp. Biol.* **206** 2547–55
- [36] Schepelmann A, Zhong Y, Austin J, Geberth K A and Geyer H 2018 Experimental evaluation of robust swing-leg placement controls in robotic limb testbeds *Technical Report CMU-RI-TR-18-62* Pittsburgh, PACarnegie Mellon University
- [37] Pratt G A and Williamson M M 1995 Series elastic actuators *Proc. 1995 IEEE/RSJ Int. Conf. on Intelligent Robots and Systems. Human Robot Interaction and Cooperative Robots* vol 1 pp 399–406 (ieeexplore.ieee.org)
- [38] Robinson D W, Pratt J E, Paluska D J and Pratt G A 1999 Series elastic actuator development for a biomimetic walking robot 1999 *IEEE/ASME Int. Conf. on Advanced Intelligent Mechatronics (Cat. No. 99TH8399)* pp 561–8 (ieeexplore.ieee.org)
- [39] Hubicki C, Grimes J, Jones M, Renjewski D, Sprowitz A, Abate A and Hurst J 2016 ATRIAS: design and validation of a tether-free 3d-capable spring-mass bipedal robot *Int. J. Robot. Res.* **35** 1497–521
- [40] Galloway K C, Clark J E and Koditschek D E 2010 Design of a tunable stiffness composite leg for dynamic locomotion *ASME 2009 Int. Design Engineering Technical Conferences and Computers and Information in Engineering Conf. (American Society of Mechanical Engineers Digital Collection)* pp 215–22
- [41] Galloway K C, Clark J E, Yim M and Koditschek D E 2011 Experimental investigations into the role of passive variable compliant legs for dynamic robotic locomotion 2011 *IEEE International Conference on Robotics and Automation* pp 1243–9 (ieeexplore.ieee.org)
- [42] Galloway K C, Clark J E and Koditschek D E 2013 Variable stiffness legs for robust, efficient, and stable dynamic running *J. Mech. Robot.* **5** 011009
- [43] Batts Z, Kim J and Yamane K 2016 Untethered one-legged hopping in 3D using linear elastic actuator in parallel (LEAP) 2016 *Int. Symp. on Experimental Robotics (Springer Proceedings in Advanced Robotics)* (Cham: Springer) pp 103–12
- [44] Tolley M T, Shepherd R F, Mosadegh B, Galloway K C, Wehner M, Karpelson M, Wood R J and Whitesides G M 2014 A resilient, untethered soft robot *Soft Robot.* **1** 213–23
- [45] Drotman D, Jadhav S, Karimi M, deZonia P and Tolley M T 2017 3D printed soft actuators for a legged robot capable of navigating unstructured terrain 2017 *IEEE Int. Conf. on Robotics and Automation (ICRA)* pp 5532–8
- [46] Blickhan R, Seyfarth A, Geyer H, Grimmer S, Wagner H and Günther M 2007 Intelligence by mechanics *Phil. Trans. R. Soc. A* **365** 199–220
- [47] Hurst J W and Rizzi A A 2005 Physically variable compliance in running *Climbing and Walking Robots* ed M A Armada and P de González Santos (Berlin: Springer) pp 123–33
- [48] Hutter M, Remy C D, Höpflinger M A and Siegwart R 2010 SLIP running with an articulated robotic leg 2010 *IEEE/RSJ Int. Conf. on Intelligent Robots and Systems* pp 4934–9
- [49] Park H, Park S and Kim S 2015 Variable-speed quadrupedal bounding using impulse planning: untethered high-speed 3D running of MIT cheetah 2 2015 *IEEE Int. Conf. on Robotics and Automation (ICRA)* pp 5163–70
- [50] Chuah M Y and Kim S 2014 Enabling force sensing during ground locomotion: a bio-inspired, multi-axis, composite force sensor using discrete pressure mapping *IEEE Sensor. J.* **14** 1693–703
- [51] Semini C, Barasuol V, Boaventura T, Frigerio M, Focchi M, Caldwell D G and Buchli J 2015 Towards versatile legged robots through active impedance control *Int. J. Robot. Res.* **34** 1003–20
- [52] Seok S, Wang A, Otten D and Kim S 2012 Actuator design for high force proprioceptive control in fast legged locomotion 2012 *IEEE/RSJ Int. Conf. on Intelligent Robots and Systems* pp 1970–5
- [53] Kenneally G, De A and Koditschek D E 2016 Design principles for a family of direct-drive legged robots *IEEE Robot. Autom. Lett.* **1** 900–7
- [54] Arm P et al 2019 SpaceBok: a dynamic legged robot for space exploration 2019 *Int. Conf. on Robotics and Automation (ICRA)* pp 6288–94
- [55] Austin M P, Brown J M, Young C A and Clark J E 2018 Leg design to enable dynamic running and climbing on BOBCAT 2018 *IEEE/RSJ Int. Conf. on Intelligent Robots and Systems (IROS)* pp 3799–806
- [56] Brown J M, Carbiener C P, Nicholson J, Hemenway N, Pusey J L and Clark J E 2018 Fore-aft leg specialization controller for a dynamic quadruped 2018 *IEEE Int. Conf. on Robotics and Automation (ICRA)* pp 4383–90
- [57] Blackman D J, Nicholson J V, Pusey J L, Austin M P, Young C, Brown J M and Clark J E 2017 Leg design for running and jumping dynamics 2017 *IEEE Int. Conf. on Robotics and Biomimetics (ROBIO)* pp 2617–23
- [58] Blackman D J, Nicholson J V, Ordonez C, Miller B D and Clark J E 2016 Gait development on minitaur, a direct drive quadrupedal robot *Unmanned Systems Technology XVIII* vol 9837 (International Society for Optics and Photonics) p 98370I
- [59] Austin M, Brown J, Geidel K, Wang W and Clark J 2017 Gait design and optimization for efficient running of a direct-drive quadrupedal robot *Unmanned Systems Technology XIX* vol 10195 (International Society for Optics and Photonics) p 1019504
- [60] Kalouche S 2017 GOAT: a legged robot with 3D agility and virtual compliance 2017 *IEEE/RSJ Int. Conf. on Intelligent Robots and Systems (IROS)* pp 4110–7
- [61] Kau N, Schultz A, Ferrante N and Slade P 2019 Stanford doggo: an open-source, quasi-direct-drive quadruped 2019 *Int. Conf. on Robotics and Automation (ICRA)* pp 6309–15
- [62] van der Walt S, Colbert S C and Varoquaux G 2011 The NumPy array: a structure for efficient numerical computation *Comput. Sci. Eng.* **13** 22–30
- [63] Virtanen P et al 2020 SciPy 1.0: fundamental algorithms for scientific computing in Python *Nat. Methods* **17** 352

- [64] Hyun D J, Seok S, Lee J and Kim S 2014 High speed trot-running: implementation of a hierarchical controller using proprioceptive impedance control on the MIT cheetah *Int. J. Robot. Res.* **33** 1417–45
- [65] Kryczka P, Kormushev P, Tsagarakis N G and Caldwell D G 2015 Online regeneration of bipedal walking gait pattern optimizing footstep placement and timing *2015 IEEE/RSJ Int. Conf. on Intelligent Robots and Systems (IROS)* pp 3352–7 (ieeexplore.ieee.org)
- [66] Kaminaga H, Engelsberger J and Ott C 2012 Kinematic optimization and online adaptation of swing foot trajectory for biped locomotion *2012 12th IEEE-RAS Int. Conf. on Humanoid Robots (Humanoids 2012)* pp 593–9 (ieeexplore.ieee.org)
- [67] Hubicki C et al 2018 Walking and running with passive compliance: lessons from engineering: a live demonstration of the ATRIAS biped *IEEE Robot. Autom. Mag.* **25** 23–39
- [68] Dudek D M and Full R J 2006 Passive mechanical properties of legs from running insects *J. Exp. Biol.* **209** 1502–15
- [69] Dudek D M and Full R J 2007 An isolated insect leg's passive recovery from dorso-ventral perturbations *J. Exp. Biol.* **210** 3209–17
- [70] Dudek D M and Full R J 2007 An isolated insect leg's passive recovery from dorso-ventral perturbations *J. Exp. Biol.* **210** 3209–17
- [71] McNeill Ingham S J, de Carvalho R T, Abdalla R J, Fu F H and Lovejoy C O 2017 Bony morphology: comparative anatomy and its importance for the anterior cruciate ligament *Operat. Tech. Orthop.* **27** 2–7
- [72] Lovejoy C O 2007 The natural history of human gait and posture *Gait Posture* **25** 325–41
- [73] Ishikawa M, Komi P V, Grey M J, Lepola V and Brüggemann G-P 2005 Muscle–tendon interaction and elastic energy usage in human walking *J. Appl. Physiol.* **99** 603–8
- [74] Biewener A A and Roberts T J 2000 Muscle and tendon contributions to force, work, and elastic energy savings: a comparative perspective *Exerc. Sport Sci. Rev.* **28** 99–107
- [75] Swartz S M and Middleton K M 2008 Biomechanics of the bat limb skeleton: scaling, material properties and mechanics *Cells Tissues Organs* **187** 59–84
- [76] Vincent J F V and Wegst U G K 2004 Design and mechanical properties of insect cuticle *Arthropod Struct. Dev.* **33** 187–99
- [77] Wootton R J 1999 Invertebrate paraxial locomotory appendages: design, deformation and control *J. Exp. Biol.* **202** 3333–45
- [78] Spagna J C, Goldman D I, Lin P-C, Koditschek D E and Full R J 2007 Distributed mechanical feedback in arthropods and robots simplifies control of rapid running on challenging terrain *Bioinspir. Biomim.* **2** 9
- [79] Gravish N, Garcia M, Mazouchova N, Levy L, Umbanhowar P B, Goodisman M A D and Goldman D I 2012 Effects of worker size on the dynamics of fire ant tunnel construction *J. R. Soc. Interface* **9** 3312–22